Physics Letters B 839 (2023) 137815

Contents lists available at ScienceDirect

Physics Letters B

journal homepage: www.elsevier.com/locate/physletb

Single-particle spectroscopic strength from nucleon transfer reactions with a three-nucleon force contribution

N.K. Timofeyuk [a,*], L. Moschini [a], M. Gómez-Ramos [b]

[a] Department of Physics, Faculty of Engineering and Physical Sciences, University of Surrey, Guildford, Surrey GU2 7XH, United Kingdom
[b] Departamento de FAMN, Universidad de Sevilla, Apartado 1065, 41080 Sevilla, Spain

ARTICLE INFO

Article history:
Received 12 October 2022
Received in revised form 25 January 2023
Accepted 27 February 2023
Available online 2 March 2023
Editor: B. Balantekin

ABSTRACT

The direct reaction theory widely used to study single-particle spectroscopic strength in nucleon transfer experiments is based on a Hamiltonian with two-nucleon interactions only. We point out that in reactions with a loosely-bound projectile, where clustering and breakup effects are important, an additional three-body force arises due to three-nucleon ($3N$) interaction between two nucleons belonging to different clusters in the projectile and a target nucleon. We study the effects of this force on nucleon transfer in (d,p) and (d,n) reactions on ^{56}Ni, ^{48}Ca, ^{26m}Al and ^{24}O targets at deuteron incident energies between 4 and 40 MeV/nucleon. Deuteron breakup is treated exactly within a continuum discretized coupled-channel approach. It was found that an additional three-body force can noticeably alter the angular distributions at forward angles, with consequences for spectroscopic factors' studies. Additional study of transfer to $2p$ continuum in the ^{25}F$(p,2p)^{24}$O reaction, involving the same overlap function as in the ^{24}O$(d,n)^{25}$F case, revealed that $3N$ force affects the (d,n) and $(p,2p)$ reactions in a similar way, increasing the cross sections and decreasing spectroscopic factors, although its influence at the main peak of $(p,2p)$ is weaker. The angle-integrated cross sections are found to be less sensitive to the 3N force contribution, they increase by less than 20%. Including 3N interactions in nucleon removal reactions makes an essential step towards bringing together nuclear structure theory, where 3N force is routinely used, and nuclear direct reaction theory, based on two-nucleon interactions only.

The spectroscopic strength of nucleon states in atomic nuclei, often associated with spectroscopic factors, is central to our understanding of nuclear structure. Due to its connections with nucleon orbit occupancy [1] it has received enormous attention for the last 60 years from the nuclear structure community. Today, the rapid progress of ab-initio treatments of nuclear structure [2] has enabled spectroscopic factors to be related to realistic forces between nucleons.

Spectroscopic factors are often determined from nucleon transfer and nucleon removal experiments by comparing measured and calculated cross sections. Over the last two decades experimental studies scrutinized spectroscopic factor uncertainties using different reaction probes, at the same time extending significantly the range of studied isotopes thanks to the increased availability of radioactive beams worldwide. The experimental studies revealed that spectroscopic factors can be significantly lower than structure model predictions even for double magic closed shell nuclei [3]. This phenomenon, named "spectroscopic-factor quenching", occurs because nucleon-nucleon (NN) correlations scatter nucleons beyond the mean-field shell model space. The most puzzling discovery from a remarkable set of data collected over two decades is the quenching dependence on neutron-proton binding asymmetry seen in inverse-kinematic nucleon knockout experiments with ^{9}Be target [4] and the absence of significant asymmetry-dependent quenching in nucleon transfers, such as (p,d) reactions [5–7]. Given that spectroscopic-factor determination heavily relies on reaction theory, the nuclear physics community agrees that nucleon-removal reaction models should be further developed and, in particular, moved towards a better integration and coherent description with modern nuclear structure theories. However, the challenges in this direction are significant.

In this Letter, we present a new step towards integrating nuclear reaction and structure theories by pointing out that analysis of all nucleon transfer and nucleon removal experiments is carried out using distorted-wave-type direct reaction models based on a Hamiltonian with NN interaction only [8]. However, it has been known since the 1950s that the three-nucleon (3N) force is important for the correct description of atomic nuclei. In reactions with

* Corresponding author.
E-mail addresses: n.timofeyuk@surrey.ac.uk (N.K. Timofeyuk), l.moschini@surrey.ac.uk (L. Moschini), mgomez40@us.es (M. Gómez-Ramos).

https://doi.org/10.1016/j.physletb.2023.137815

loosely-bound projectiles, where clustering and breakup effects are important, the 3N interaction between two nucleons belonging to different clusters in the projectile and a target nucleon creates an additional three-body force [9]. We aim to understand if this novel force can give any noticeable effect on nucleon transfer cross sections so that that could eventually contribute to resolving the puzzling contradiction in spectroscopic factors quenching deduced from transfer and knockout experiments. We choose the deuteron as an example of a loosely-bound projectile and consider (d,p) and (d,n) reactions – a popular tool choice for spectroscopic factor studies. Due to the small binding energy of 2.2 MeV the deuteron breaks up easily into neutron n and proton p when interacting with a target, invoking a need for a three-body treatment of its motion before transfer. In addition, we study one case of a popular alternative to knockout experiments with heavy ions – $(p,2p)$ – where the two final protons are in the continuum and the three-body description of the final state is mandatory.

We consider an n-p-A model for d-A scattering, where A is the target, taking the n-A and p-A interactions U_{nA} and U_{pA} from optical model, and add to the three-body Hamiltonian a 3N-induced contribution $\langle\phi_A|\sum_j W_{jnp}|\phi_A\rangle$, where ϕ_A is the target wave function and W_{jnp} is the 3N interaction of target nucleon j with neutron n and proton p from deuteron. We solve the n-p-A problem in the continuum-discretized coupled-channel (CDCC) approach [10,11]. This requires constructing continuum bins ϕ_i from n-p scattering wave functions and calculating the matrix elements $U_{3N}^{(ii')}(\boldsymbol{R}) = \langle\phi_i\phi_A|\sum_j W_{jnp}|\phi_A\phi_{i'}\rangle$ (or coupling potentials) which are function of the coordinate $\boldsymbol{R}$ connecting the n-p centre of mass with the target A. The radial part of these matrix elements could be read into a CDCC reaction code, which in our case was FRESCO [12], to supplement the coupling potentials $U_{\rm opt}^{(ii')}(\boldsymbol{R}) = \langle\phi_A\phi_i|U_{pA}+U_{nA}|\phi_A\phi_{i'}\rangle$ arising from optical n-A and p-A interactions. To develop $U_{3N}^{ii'}(\boldsymbol{R})$, we first calculate the effective transition interaction $\tilde{W}_{dj}^{(ii')} = \langle\phi_i^{I_d m_d}|W_{jnp}|\phi_{i'}^{I'_d m'_d}\rangle$ connecting initial and final bin states of the n-p pair with the nucleon j belonging to the target A. We express it using a standard partial wave decomposition:

$$\langle\phi_i^{I_d m_d}|W_{jnp}|\phi_{i'}^{I'_d m'_d}\rangle = \sqrt{4\pi}\sum_{\lambda I_d I'_d}\tilde{W}^{(ii')}_{\lambda I_d I'_d}(r_{dj})(\lambda\mu I'_d m'_d|I_d m_d)Y^*_{\lambda\mu}(\hat{\mathbf{r}}_{di}), \quad (1)$$

where I_d and m_d are the total angular momentum and its projection of bin i, the coordinate r_{di} connects the n-p centre of mass and target nucleon j and Y is the spherical function. The d-j interaction is then folded with the target density ρ_A to obtain the radial part $U^{(ii')}_{\lambda I_d I'_d}(R)$ of the coupling potential $U_{3N}^{ii'}(\boldsymbol{R})$:

$$U^{(ii')}_{\lambda I_d I'_d}(R) = 4\pi(-)^{I_d-I'_d}(2\lambda+1)(2I'_d+1) \times\int_0^\infty dr_{dj} r_{dj}^2\rho_\lambda(r_{dj},R)\tilde{W}^{(ii')}_{\lambda I_d I'_d}(r_{dj}), \quad (2)$$

where it was assumed that the target A is spherical so that

$$\rho_\lambda(r_{dj},R) = \frac{1}{2}\int_{-1}^{1} d\mu\, P_\lambda(\mu)\rho_A\left(|\boldsymbol{r}_{dj}-\boldsymbol{R}|\right), \quad (3)$$

and $P_\lambda(\mu)$ are the Legendre polynomials.

The effective potential $\tilde{W}_{dj}^{(ii')}$ is determined by the strength of W_{jnp} and by the n-p wave functions behaviour within its short range, thus requiring a consistent choice of the NN and 3N interactions. Today, the most popular consistent choice of NN+3N interactions is provided by the chiral effective field theory (χEFT) [13]. However, we are not yet in a position to use it because most χEFT potentials are nonlocal while the CDCC can only handle local interactions. In addition, the spin-isospin structure of the χEFT operators (both nonlocal and a few available local ones) requires knowledge of the spin density distributions in the target A, which is not yet available. Therefore, we choose a phenomenological NN force AV18 [14] supplemented by Urbana IX (UIX) interaction [15] – a combination successfully used in ab-initio Green's Function Monte Carlo calculations of light nuclei [16] and scattering studies in few-body systems [17–19]. The UIX potential consists of a contact and 2π-exchange terms and the formal derivation of (rather cumbersome) expressions for $\tilde{W}_{dj}^{(ii')}$ involving these contributions is given in Supplement for targets with spin 0^+.

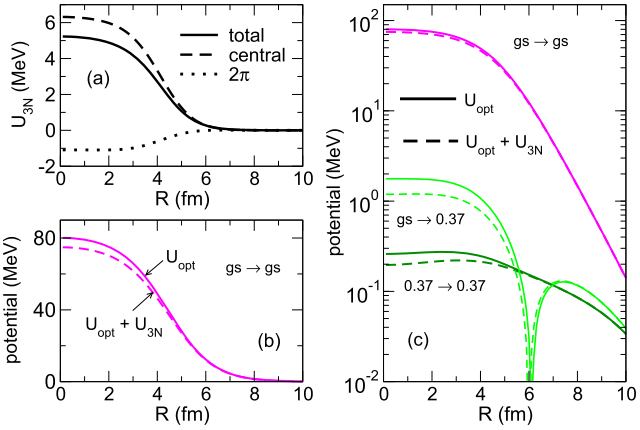

Fig. 1. (a) U_{3N}^{00} potential for d+^{56}Ni calculated with contact (dashed line), 2π-exchange (dotted line) contributions and their sum (solid line). (b) Absolute values of $U_{\rm opt}^{ii'}$ (solid lines) and its sum with $U_{3N}^{ii'}$ (dashed lines) for $i=i'=0$, (c) the same as (b) for two diagonal and one non-diagonal cases, using deuteron ground state and a low-energy 1^+ bin centred at 0.37 MeV. $U_{\rm opt}^{ii'}$ has been calculated for $d+^{56}$Ni at $E_d = 32$ MeV/nucleon.

The following zero-spin targets are considered here: ^{48}Ca, ^{56}Ni, ^{26m}Al and ^{24}O. The densities of the first three of them were taken from a compilation [20] of charge densities extracted from electron scattering. We assumed that symmetrical $N=Z$ nuclei ^{56}Ni and ^{26m}Al have the same proton and nucleon density distributions while in ^{48}Ca they are proportional to each other. For ^{24}O three different models were used: renormalised ^{18}O harmonic-oscillator from [20], the ^{24}O Hartree-Fock with SkM interaction and the SkM-Hartree-Fock ^{22}O-core density plus valence-nucleon-density from Gamow shell model of [21]. For all four isotopes different choices of the target density did not affect the final cross sections.

Fig. 1 shows typical CDCC potentials $U_{3N}^{ii'}(R)$ for a case of d+^{56}Ni. The $U_{3N}^{(00)}$, corresponding to the deuteron ground state, is repulsive with the strength of 5.1 MeV, determined mostly by the UIX contact part (Fig. 1a). The 2π-exchange gives a small attractive contribution with the depth of 1.26 MeV coming mainly from the deuteron d-state. Fig. 1b,c show CDCC diagonal and non-diagonal optical coupling potentials $U_{\rm opt}^{(ii')}(R)$ and their sums with $U_{3N}^{(ii')}$ for deuteron ground state and low-energy 1^+ bin centred at 0.37 MeV.

To carry out finite-range CDCC calculations we modified computer code FRESCO by including the NN potential AV18 (taken from [22]) to generate the ϕ_i bins. We made sure that the n-p scattering functions published in [22] were reproduced. Both s- and d-wave continuum bins were used in (d,p) and (d,n) calculations. The number of bins was the same for each component. The bins were evenly distributed between 0 and some maximum n-p

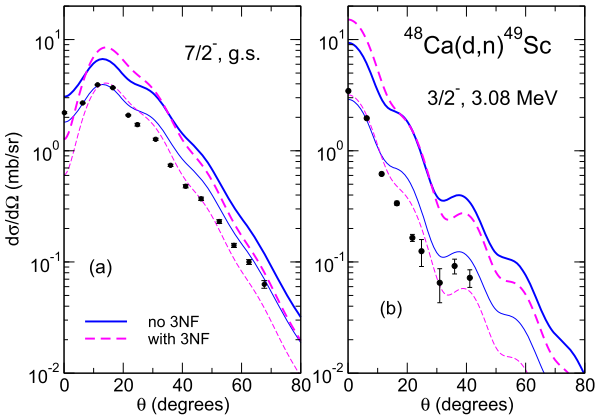

Fig. 2. The ^{48}Ca$(d,n)^{49}$Sc angular distributions at $E_d = 40$ MeV/nucleon for (a) the ground and (b) first excited ^{49}Sc states, calculated in CDCC with (dashed) and without (solid) $U_{3N}^{(ii')}$ assuming $S = 1$ (thick lines). Thin lines show CDCC cross sections renormalized to experimental data from [26].

energy which was 8.7, 46, 59 and 72 MeV for $E_d = 4.6$, 25, 32 and 40 MeV/nucleon, respectively. The corresponding bin numbers were 3, 12, 20 and 18. Convergence with bin size and numbers was checked at all energies and was found be the same as for any CDCC calculations, not being affected by inclusion of the 3N force. The n-A and p-A optical potentials were taken from widely used Koening-Delaroche global systematics [23]. The transferred nucleon bound-state wave functions were obtained from a two-body potential model of the standard geometry (radius $r_0 = 1.25$ fm and diffuseness $a = 0.65$ fm), except for ^{48}Ca where $r_0 = 1.33$ fm was used. Prior to calculations with 3N force, we made a few standard CDCC runs with a reduced real part of the optical potentials to simulate 3N effects. We found that even small changes, about 5%, can noticeably affect (d,p) cross sections. We calculated two types of observables: angular distributions, commonly used in spectroscopic factor studies, and angle-integrated cross sections. The latter have been measured recently for excited final states populated in (d,n) reactions via their γ-de-excitation [24]. The motivation for such experiments comes from the need in nuclear data for nuclear astrophysics [25].

We start with ^{48}Ca$(d,n)^{49}$Sc reaction at $E_d = 40$ MeV/nucleon, measured in [26], populating the lowest single-particle proton states $7/2^-$ and $3/2^-$ above the double-closed-shell stable nucleus ^{48}Ca. According to Independent Particle Model (IPM), their spectroscopic factors S should be one. However, accounting for NN correlations in Self-Consistent Green's Functions (SCGF) method [27] and Source-Term Approach (STA) [28] predicts significantly smaller values, $S \sim 0.5 - 0.7$. The proton and neutron separation energies in ^{49}Sc are similar and in this case the spectroscopic factors from knockout experiments are typically 45-75% of the IPM and/or shell model predictions. The distorted-wave Born approximation (DWBA) and adiabatic distorted wave approximation (ADWA) analysis of ^{48}Ca$(d,n)^{49}$Sc, conducted in [26], have also indicated a similar quenching for $7/2^-$ state, with $S \sim 0.6$ and 0.7, respectively, and a more significant quenching for $3/2^-$, with $S \sim 0.25$ and 0.31. However, treating deuteron breakup beyond the adiabatic approximation in CDCC with the same optical potentials (taken from Becchetti-Greenless systematics [29]) resulted in a poor match between calculated and experimental angular distributions, making spectroscopic factor extraction meaningless. We found that CDCC with Koening-Delaroche potentials gives a better match between predictions and the experimental data of [26], further improved by adding the 3N contribution. Fig. 2 shows CDCC calculations with $S = 1$ by thick lines while thin lines are the same calculations multiplied by S values from Table 1. The 3N contribution reduces spectroscopic factors for ^{49}Sc(g.s.) and ^{49}Sc$^*(3/2^-)$ by 23% and

Table 1
Spectroscopic factors from CDCC analysis of angle-integrated (for ^{56}Ni) and differential (for ^{48}Ca) cross sections with and without 3N force, in comparison with other values from literature.

Reaction	no 3NF	with 3NF	Literature
^{48}Ca$(d,n)^{49}$Sc$(g.s.)$	0.59	0.48 (0.90)[g]	0.61[e]; 0.72[f] 0.73[c]; 0.61[d]
^{48}Ca$(d,n)^{49}$Sc*(3.08)	0.31	0.21 (0.39)[g]	0.25[e]; 0.31[f] 0.48[c]; 0.55[d]
^{56}Ni$(d,p)^{57}$Ni*(0.768)	0.78(22)	0.72(21)	0.77(31)[a]; 0.74[b]; 0.55[c]; 0.68[d]
^{26m}Al$(d,p)^{27}$Al*(0.84)	0.10(2)	0.09(2)	0.08(3)[h]; 0.11-0.13[i]
^{26m}Al$(d,p)^{27}$Al*(6.8)	0.13(2)	0.13(2)	0.11(3)[h]; 0.14[i]

[a] ADWA analysis in [24].
[b] Shell model calculations [24].
[c] Theoretical values from SCGF [27,32].
[d] STA values recalculated here using updated harmonic oscillator radii as suggested in [33].
[e] DWBA analysis in [26].
[f] ADWA analysis in [26].
[g] Becchetti-Greenless optical potential systematics.
[h] DWBA and ADWA analysis in [36].
[i] Leading order nonlocal CDCC analysis in [34].

47%, respectively, mainly due to a noticeable change of the angular distribution's shape in the area most important for spectroscopic factor determination. These spectroscopic factors show a more significant quenching than that predicted by SCGF and STA, especially for the excited ^{49}Sc$^*(3/2^-)$ state.

We proceed with another double-closed-shell target ^{56}Ni, close to stability but radioactive, adding neutron or proton to it in (d,p) and (d,n) reactions. The final mirror ^{57}Ni$(3/2^-)$ and ^{57}Cu$(3/2^-)$ ground states have very different valence neutron and proton separation energies, 10.248 and 0.690 MeV, respectively, and a very large difference in neutron and proton binding, +3 and -16.5 MeV. The systematic from [4] suggests $S \sim 1$ could be expected for ^{57}Cu, while the $S_{\rm exp} = 0.58(11)$ value was derived from neutron knockout in [30]. The pf shell model gives $S = 0.91$ for ^{57}Ni [31], close to the IPM value, but SCGF and STA predict significantly lower values of 0.65 [32] and 0.59 [28], respectively, in agreement with knockout experiment. Similar values, $S = 0.67$ and 0.70, are predicted for ^{57}Cu both by SCGF [32] and STA [28], suggesting no strong asymmetry-dependent quenching. When choosing these two mirror reactions we expected the 3N contribution would be more important in ^{57}Ni than in ^{57}Cu because rapidly decreasing neutron wave function outside ^{56}Ni could amplify contributions from small d-^{56}Ni separations in the entrance channel wave function, facilitating the 3N interaction to occur. However, our calculations at the energy $E_d = 32$ MeV/nucleon, used in experiments with ^{56}Ni beam [24], show comparable 3N effects in mirror ^{56}Ni$(d,p)^{57}$Ni and ^{56}Ni$(d,n)^{57}$Cu reactions (see Fig. 3a), suggesting that they will not affect the asymmetry-quenching problem. Depending on angles, they either increase or decrease the differential cross section so that interpretation of experimental data will depend on the angular range accessible to measurements. A similar picture occurs for (d,p) reaction populating ^{57}Ni excited states $\frac{5}{2}^-$ at 0.768 MeV and $\frac{9}{2}^+$ at 3 MeV (see Fig. 3b). The angle-integrated cross section $\sigma_{\rm AI} = 2.10(60)$ mb for the first $\frac{5}{2}^-$ state has been measured in [24], motivated by its important role in understanding the pr process in stars, with the ADWA analysis giving $S = 0.77(31)$. Based on our CDCC results for $\sigma_{\rm AI}$, collected in Table 2, we obtained $S = 0.78(22)$ and 0.72(21) without and with 3N force, respectively.

The two above examples were shown for deuteron incident energies in the 30-40 MeV/nucleon region assuming that 3N effects could be especially noticeable at high deuteron energies. Many radioactive beam facilities operate at lower energies, 5-10 MeV/nucleon, where deuteron breakup can be important too [35]. We have assessed the 3N role at 4.6 MeV/nucleon for ^{26m}Al$(d,p)^{27}$Al reac-

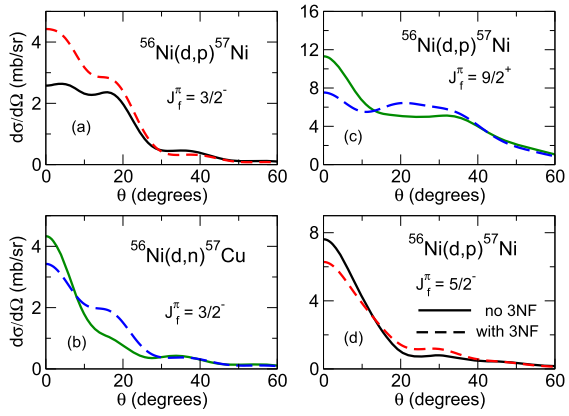

Fig. 3. The CDCC angular distributions for (a) ^{56}Ni$(d,p)^{57}$Ni(g.s.), (b) ^{56}Ni$(d,n)^{57}$Cu(g.s.) as well as (c, d) ^{56}Ni$(d,p)^{57}$Ni$(\frac{5}{2}^-, \frac{9}{2}^+)$ reactions at $E_d = 32$ MeV/nucleon obtained with (dashed lines) and without (solid lines) $U^{(ii')}_{3N}$.

Table 2
Angle-integrated cross sections $\sigma_{\rm Al}$ (in mb) for reactions from first column calculated without and with $U^{(ii')}_{3N}$ assuming $S = 1$. The valence nucleon quantum numbers lj and the incident laboratory energy (in MeV/nucleon) are in second and third columns, respectively, and the change with adding $U^{(ii')}_{3N}$ is indicated in the last column. For $(p,2p)$ reaction E refers to three-body p+p+^{24}O final state energy.

Reaction	lj	E_d	no 3NF	with 3NF	change
^{56}Ni$(d,p)^{57}$Ni$(g.s.)$	$p_{3/2}$	32	2.002	2.211	+11%
^{56}Ni$(d,n)^{57}$Cu$(g.s.)$	$p_{3/2}$	32	1.432	1.699	+19%
^{56}Ni$(d,p)^{57}$Ni*(0.768)	$f_{5/2}$	32	2.698	2.923	+8%
^{56}Ni$(d,p)^{57}$Ni*(3.09)	$g_{9/2}$	32	12.70	12.80	+1%
^{48}Ca$(d,n)^{49}$Sc$(g.s.)$	$f_{7/2}$	40	6.799	7.376	+8%
^{48}Ca$(d,n)^{49}$Sc*(3.08)	$p_{3/2}$	40	2.211	2.490	+13%
^{26m}Al$(d,p)^{27}$Al$(g.s.)$	$d_{5/2}$	4.6	19.27	23.25	+21%
^{26m}Al$(d,p)^{27}$Al*(0.84)	$s_{1/2}$	4.6	16.91	20.35	+20%
^{26m}Al$(d,p)^{27}$Al*(6.8)	$s_{1/2}$	4.6	31.48	32.70	+4%
^{24}O$(d,n)^{25}$F$(g.s.)$	$d_{5/2}$	25	13.49	14.44	+7%
^{24}O$(d,n)^{25}$F*(0.495)	$s_{1/2}$	25	5.043	5.587	+11%
^{25}F$(p,2p)^{24}$O$(g.s.)$	$d_{5/2}$	25	1.287	1.382	+7%
^{25}F$(p,2p)^{24}$O$(g.s.)$	$s_{1/2}$	25	1.989	2.138	+7%

tion studied in [36] as a surrogate for the proton capture reaction ^{26m}Al$(p,\gamma)^{27}$Si – a major destruction pathway of ^{26}Al, in Wolf-Rayet and AGB stars [37]. Fig. 4 shows angular distributions for populating the ground $5/2^+$ state and two excited $1/2^+$ states, at $E_x = 0.84$ and 6.8 MeV. For $l = 2$ transfer to the ground state the 3N effects increase the main peak cross section by 12% but in the $l = 0$ case this increase is 8% and 5% for $E_x = 0.84$ and 6.8 MeV, respectively, affecting the lowest state with a stronger bound energy more, as expected. The spectroscopic factors, collected in Table 1, are slightly reduced in the 0.84 MeV case but, in general, are within limits of all previous analyses. The angle-integrated cross sections are more affected by 3N contribution, about 20% for the lowest $1/2^+$ state with larger separation energy while the state at 6.8 MeV is almost unaffected (see Table 2).

Finally, we consider two complementary reactions, ^{24}O$(d,n)^{25}$F and ^{25}F$(p,2p)^{24}$O, involving the same strongly-bound (by 14 MeV) single-proton state above a double-closed shell nucleus ^{24}O with large neutron-proton asymmetry. The spectroscopic factor quenching in ^{25}F has been reported in [38] where it was measured from a quasi-free $(p,2p)$ reaction at 270 MeV/nucleon providing a value of 0.36(13), in agreement with the STA prediction of 0.46 [28] within error bars. Based on many spectroscopic factor compilations from transfer reactions [3,39,40,6], one can anticipate a larger value from future ^{24}O$(d,n)^{25}$F experiments. Here we want to check if 3N force manifestation in (d,n) and $(p,2p)$ is the same

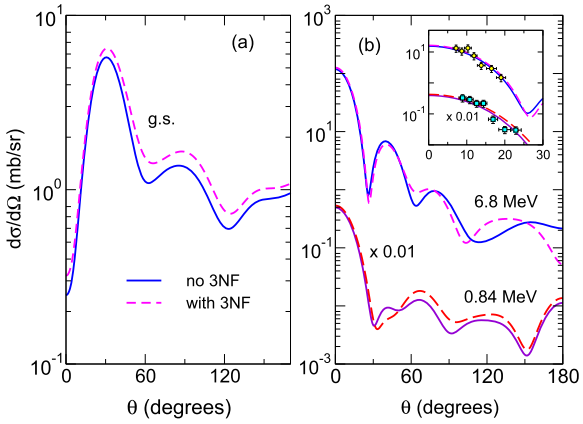

Fig. 4. The CDCC angular distributions for ^{26m}Al$(d,p)^{27}$Al at $E_d = 4.6$ MeV/nucleon populating (a) the ground $J^\pi_f = 5/2^+$ and (b) excited $J^\pi_f = 1/2^+$ states at $E_x = 0.84$ and 6.8 MeV, calculated with (dashed) and without (solid) $U^{(ii')}_{3N}$ for $S = 1$. The inset shows the same calculations for $1/2^+$ state renormalised by 0.07 and 0.13 for $E_x = 0.84$ and 6.8 MeV, respectively, in comparison with experimental data from [36].

or not. To make sure that any possible differences do not come from different kinematic conditions, we carry out calculations at the same energy in the d+^{24}O and ^{24}O+p+p channels, 25 MeV/nucleon, available for (d,n) experiments in GANIL, NSCL, JINR, and plot the same observables – the angular distributions. The corresponding p+^{25}F energy for $(p,2p)$ experiment is 32 MeV/nucleon, available at NSCL. At the energy chosen, the $(p,2p)$ mechanism can be well described by transfer to the $2p$ continuum [41] and treated within the CDCC.

The $U^{(ii')}_{3N}$ potentials for the $2p$-A and d-A systems are found to be similar, being repulsive and mainly determined by the contact interaction. Unlike in the d-A case, the 2π-exchange contribution in $(p,2p)$ is repulsive, being negligible in the nuclear interior but noticeable at the surface. In CDCC calculations of $(p,2p)$ reactions, we included contributions from s- and p-wave $2p$ continuum, which dominates in $(p,2p)$ reactions. Convergence has achieved with 15 bins for each component, evenly distributed between 0 and 41 MeV. To check the 3N effect dependence on valence proton quantum numbers we populate the ground ^{25}F$(\frac{5}{2}^+)$ state and not yet observed and experimentally unachievable for $(p,2p)$ reactions excited ^{25}F$(\frac{1}{2}^+)$ state assuming that s-wave proton energy is the same as in ^{17}F$(\frac{1}{2}^+)$.

The ^{24}O$(d,n)^{25}$F and ^{25}F$(p,2p)^{24}$O differential cross sections, obtained in CDCC with and without 3N force, are shown in Fig. 5. The 3N effects increase the (d,n) main peak cross sections by 23% and 35% for $5/2^+$ and $1/2^+$, respectively, but in $(p,2p)$ they are less pronounced, being 8% and 18%. This means that the 3N-induced difference in spectroscopic factors, obtained in complementary (d,n) and $(p,2p)$ reactions from forward angles cross sections, could reach 14%. The angle-integrated cross sections are in general less affected by the 3N force (see Table 2) but this influence depends on the $2p$ bin energy, which is illustrated in Fig. 5c for $\sigma_{\rm Al}$ calculated for transitions to individual continuum bins. This means that exclusive cross section measurements corresponding to kinematically different observations may show different 3N effects thus potentially becoming a new tool for their study. Also, in all cases 3N effects were very well simulated by a simple 5% reduction of the real parts of proton-target optical potentials in the $2p$ channel.

Summarizing, we investigated if an additional force arising due to 3N interactions between neutron and proton in incoming deuteron with a target nucleon can give any effect on (d,p) and (d,n) reaction observables measured at 4-40 MeV/nucleon. We

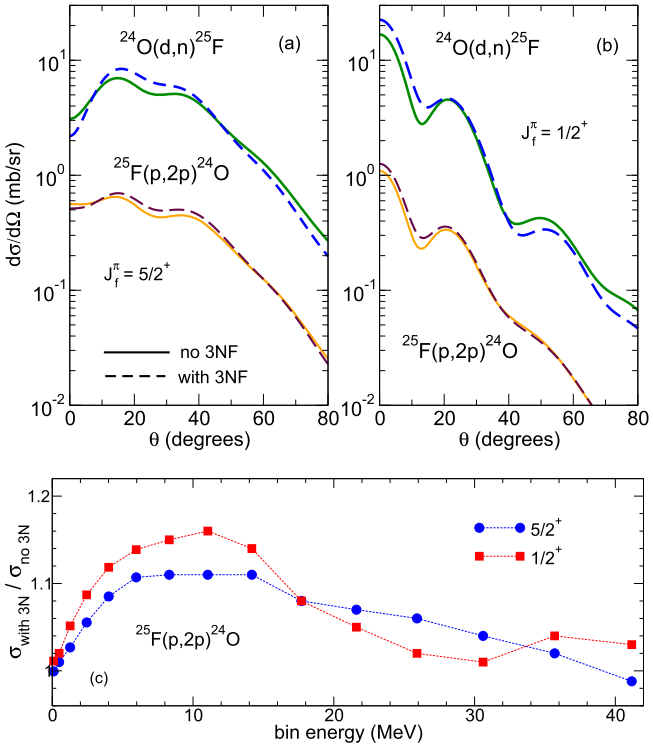

Fig. 5. The CDCC angular distributions for ^{24}O$(d,n)^{25}$F and ^{25}F$(p,2p)^{24}$O reactions at $E_d = E_{2p} = 50$ MeV populating (or knocking a nucleon from) (a) ^{25}F(g.s.) and (b) ^{25}F$^*(1/2^+)$ states, calculated with (dashed) and without (solid) $U^{(ii')}_{3N}$. Plot (c) shows ratio of $\sigma_{\rm a.i.}$ for ^{25}F$(p,2p)^{24}$O reaction for each individual $2p$ bin obtained with and without $U^{(ii')}_{3N}$.

found that this effect is noticeable, especially at $E > 20$ MeV/nucleon, where it can significantly alter the shape of angular distributions for $l \neq 0$ transfers. For $l = 0$ transfers the forward-angle angular distributions are not much affected but their absolute values can increase up to 35%, with consequences for spectroscopic factors' study. The angle-integrated cross sections, which are more sensitive to different reaction mechanisms, are less affected by 3N force, increasing by no more than by 20%. The spectroscopic factors extracted from such observables can decrease in the same proportions. Simultaneous consideration of ^{25}F$(p,2p)^{24}$O and ^{24}O$(d,n)^{25}$F reactions at the same energy in the three-body channel showed that, without 3N contributions included in the analysis, their spectroscopic factors could differ by 14%, which does contribute towards understanding the quenching-asymmetry problem. We must note that these conclusions have been made ignoring other uncertainties associated with (d,p), (d,n) and $(p,2p)$ reactions, described for example in [7,42], and using a fixed set of all reaction parameters, such as optical potentials. However, a different optical potential choice, Becchetti-Greenless, gave a similar picture here and, as shown before in [5,6] does not affect asymmetry-dependence of quenching. We must also note that choosing AV18+UIX interaction model and zero-spin targets avoided complications due to the need for unknown density components. The additional n-p-A force due to 3N contribution is very sensitive to the short-range parts of the NN scattering wave functions and 3N force so that further investigation involving other interaction models is needed. Future work will benefit from a close collaboration with structure theorists who can deliver missing nuclear density distributions consistent with a chosen NN+3N model. This will enable advanced single-particle spectroscopic strength studies for any nucleus thus helping to bring nuclear structure and nuclear reactions studies together.

Declaration of competing interest

The authors declare that they have no known competing financial interests or personal relationships that could have appeared to influence the work reported in this paper.

Data availability

The article uses widely available code and published data for input (all referenced within the paper). The code for evaluating CDCC coupling potentials induced by the 3N force can be provided on request.

Acknowledgements

We are grateful Jianguo Li for providing Gamow Shell model valence nucleon densities of ^{24}O. This work was supported by the United Kingdom Science and Technology Facilities Council (STFC) under Grants No. ST/L005743/1 and ST/V001108/1 and by Leverhulme Trust Grant No. RPG-2019-325. M.G.R. acknowledges financial support by MCIN/AEI/10.13039/501100011033 under I+D+i project No. PID2020-114687GB-I00, by the Consejería de Economía, Conocimiento, Empresas y Universidad, Junta de Andalucía (Spain) and "ERDF-A Way of Making Europe" under PAIDI 2020 project No. P20_01247, and by the European Social Fund and Junta de Andalucía (PAIDI 2020) under grant number DOC-01006. The data underlying this article are available in the article.

Appendix A. Supplementary material

Supplementary material related to this article can be found online at https://doi.org/10.1016/j.physletb.2023.137815.

References

[1] M.H. Macfarlane, J.B. French, Rev. Mod. Phys. 32 (1960) 567.
[2] H. Herbert, A guided tour of ab-initio nuclear many-body theory, Front. Phys. 8 (2020) 379.
[3] G.J. Kramer, H.P. Blok, L. Lapikás, Nucl. Phys. A 679 (3–4) (2001) 267.
[4] J.A. Tostevin, A. Gade, Phys. Rev. C 103 (2021) 054610.
[5] F. Flavigny, et al., Phys. Rev. C 97 (2018) 034601.
[6] J. Manfredi, et al., Phys. Rev. C 104 (2021) 024608.
[7] T. Aumann, et al., Prog. Part. Nucl. Phys. 118 (2021) 103847.
[8] G.R. Satchler, Direct Nuclear Reactions, Oxford University Press, New York, 1983.
[9] N.K. Timofeyuk, M.J. Dinmore, J.S. Al-Khalili, Phys. Rev. C 102 (2020) 064616.
[10] G.H. Rawitscher, Phys. Rev. C 9 (1974) 2210.
[11] N. Austern, et al., Phys. Rep. 154 (1987) 125.
[12] I.J. Thompson, Comput. Phys. Rep. 7 (1988) 167.
[13] R. Machleidt, D.R. Entem, Phys. Rep. 503 (2011) 1.
[14] R.B. Wiringa, V.G.J. Stoks, R. Schiavilla, Phys. Rev. C 51 (1995) 38.
[15] B.S. Pudliner, et al., Phys. Rev. Lett. 74 (1995) 4396.
[16] B.S. Pudliner, et al., Phys. Rev. C 56 (1997) 1720.
[17] A. Kievsky, M. Viviani, S. Rosati, Phys. Rev. C 52 (1995) R15.
[18] M. Viviani, R. Schiavilla, A. Kievsky, Phys. Rev. C 54 (1996) 534.
[19] M. Viviani, S. Rosati, A. Kievsky, Phys. Rev. Lett. 81 (1998) 1580.
[20] H. De Vries, C.W. De Jager, C. De Vries, At. Data Nucl. Data Tables 36 (1987) 495.
[21] J.G. Li, N. Michel, W. Zuo, F.R. Xu, Phys. Rev. C 103 (2021) 034305.
[22] R.B. Wiringa, https://www.phy.anl.gov/theory/research/av18/av18pot.f.
[23] A.J. Koning, J.P. Delaroche, Nucl. Phys. A 713 (2003) 23.
[24] D. Kahl, et al., Phys. Lett. B 797 (2019) 134803.
[25] R.K. Wallace, S.E. Woosley, Astrophys. J. Suppl. Ser. 45 (1981) 389.
[26] J.W. Watson, et al., Phys. Rev. C 40 (1989) 570.
[27] C. Barbieri, Phys. Rev. Lett. 103 (2009) 202502.
[28] N.K. Timofeyuk, Phys. Rev. C 84 (2011) 054313.
[29] F.D. Becchetti, G.W. Greenless, Phys. Rev. 182 (1969) 1190.
[30] K.L. Yurkewicz, et al., Phys. Rev. C 74 (2006) 024304.
[31] K.E. Rehm, et al., Phys. Rev. Lett. 80 (1998) 676.
[32] C. Barbieri, M. Hjorth-Jensen, Phys. Rev. C 79 (2009) 064313.
[33] N.K. Timofeyuk, J. Phys. G 48 (2021) 015105.
[34] M. Gómez-Ramos, N.K. Timofeyuk, Phys. Rev. C 98 (2018) 011601(R).
[35] D.Y. Pang, A.M. Mukhamedzhanov, Phys. Rev. C 90 (2014) 044611.

[36] S. Almaraz-Calderon, et al., Phys. Rev. Lett. 119 (2017) 072701.
[37] G. Lotay, et al., Phys. Rev. C 80 (2009) 055802.
[38] T.L. Tang, et al., Phys. Rev. Lett. 124 (2020) 212502.
[39] M.B. Tsang, J. Lee, W.G. Lynch, Phys. Rev. Lett. 95 (2005) 222501.
[40] B.P. Kay, J.P. Schiffer, S.J. Freeman, Phys. Rev. Lett. 111 (2013) 42502.
[41] A.M. Moro, Phys. Rev. C 92 (2015) 044605.
[42] N.K. Timofeyuk, R.C. Johnson, Prog. Part. Nucl. Phys. 111 (2020) 103738.